17th Australasian Fluid Mechanics Conference
Auckland, New Zealand
5-9 December 2010

An Investigation Into the Effects of Highly Directional Surface Roughness on Turbulent Boundary Layers

B.Nugroho, V.Kulandaivelu, Z.Harun, N.Hutchins, and J.P. Monty

Department of Mechanical Engineering
The University of Melbourne, Victoria, 3010, Australia

Abstract

The development of a zero pressure gradient turbulent boundary layer over a diverging and converging riblet arrangement is investigated experimentally. Such surface patterns are inspired by the very interesting work of Koeltzsch *et al* (6). Hot-wire studies show that these small, highly-ordered surface roughness patterns impose a high degree of three-dimensionality onto the boundary layer, causing a 100% variation in boundary layer thickness across the spanwise wavelength of the surface pattern (this, despite the fact, that the roughness height is less than 1% of the unperturbed boundary layer thickness). Detailed boundary layer traverses reveal that the local velocity above the diverging region is higher than the converging region. These results, together with turbulence intensity and energy spectra data, lead us to propose that these surface patterns have induced a large-scale counter-rotating vortex pattern into the boundary layer. Under this hypothesis, the observed three-dimensionality is primarily a result of the redistribution of turbulent profiles due to these secondary flows.

Introduction

In the last three decades the effect of highly ordered and directional surface roughness on turbulent boundary layers has attracted considerable attention. One very interesting example of such a surface is riblet-type roughness, which has been extensively studied due to its ability to reduce skin friction (see for example Berchert *et al*. (1); Bechert *et al* (2) ;Choi (3)). Riblets are essentially a series of continuous streamwise aligned grooves, typically of very small geometry. Following a thorough review of riblet investigations, Walsh (9) states that in order to attain skin friction reduction, the riblets should have a spanwise spacing $s^+ < 30$ and a wall-normal height $h^+ < 25$. Here s is spanwise spacing between riblets and h is the wall-normal distance between the peak and the trough of the riblet. The superscript $^+$ denotes viscous scaling (i.e. $s^+ = sU_\tau/\nu$, where U_τ is the friction velocity and ν is the kinematic viscosity).Further investigation by Bechert *et al*. (2) states that optimum skin friction reduction occurs when $h \geq 0.5s$. This study is motivated by more recent work by Koeltzsch *et al* (6) who show that diverging-converging arrangements of riblets within a pipe flow facility can impose large scale modifications to the local mean velocity and turbulent intensities in the logarithmic region of the flow. Inspired by these findings, the aim of this experiment is to parametrically study the effect of diverging and converging riblet arrangements on zero pressure gradient turbulent boundary layers.

Wind Tunnel Facility

The experiments were performed in an open-return blower wind tunnel located in the Walter Basset Laboratory at The University of Melbourne. The wind tunnel has a three-dimensional contraction of area ratio 8.9:1, leading into a working section with cross-sectional area 0.94 x 0.375 m and overall length 6.7 m. The roof of the wind tunnel is fully adjustable to enable accurate adjustment of the pressure gradient. These measurements were performed in a zero pressure gradient (ZPG), fully developed turbulent boundary layer (the pressure gradient was adjusted so that coefficient of pressure C_p is within ± 0.01 throughout the working section). Measurements were performed 2.9 m downstream of the inlet to the working section.

Surface Roughness

Figure 1 gives a schematic of the converging/diverging riblet arrangement employed in these experiments. A three-axis high precision CNC machine (*CNC-Technik HEIZ S-1000*) was used to create a master tile of the diverging-converging riblet pattern in acetal copolymer. The riblets were cut using a 60° tool-bit with spanwise riblet spacing $s = 0.675$ mm and height $h = 0.5$ mm (to attain $s^+ = 23$ and $h^+ = 17$). The riblets are yawed at $\alpha = \pm 30^\circ$ to the mean flow direction (see figure 1 for a definition of angle α). This angle was chosen to be less aggressive than the 45° used by Koeltzsch *et al* (6). The width of each converging and diverging region is 0.074 m (such that the repeating spanwise wavelength $\Lambda = 0.148$ m). The master tile has dimensions 0.515×0.296 m which contains two strips at $+30^\circ$ and two strips at -30° (as shown in figure 1). A mold of this tile was produced in silicone rubber and used to cast multiple polyurethane reproductions of the original tile. The resulting casts were then affixed to the floor of boundary layer wind tunnel from the beginning of the working section up to 3.09m.

Experimental set up

The tunnel was operated at a free stream velocity $U_\infty = 15$ m/s. With a hydrodynamically smooth surface, this would yield a friction Reynolds number of $Re_\tau \simeq 1900$ (where $Re_\tau = \delta U_\tau/\nu$ and δ is the boundary layer thickness). The free stream Turbulence level was $\sqrt{\overline{u^2}}/U_\infty = 1.98 \times 10^{-3}$. An automated two axis traverse (capable of moving in the spanwise and wall-normal directions) was used to obtain hot-wire measurements over a spanwise / wall-normal grid. This grid covers one complete wavelength (Λ) of the diverging-converging surface roughness pattern in the spanwise direction and 0.12 m (more than twice the boundary layer thickness for the smooth wall case) in the wall-normal direction. The wall-normal grid spacing is logarithmic. The spanwise wavelength selected is indicated by the dimension Λ in figure 1, with a diverging arrangement (labeled ② in figure 1) at the spanwise center of the measurement domain, and converging patterns at the edges (① and ③).

Measurements were performed using a single-normal hot-wire probe operated at constant temperature using an *AA Lab System AN-1003* anemometer (with overheat ratio set to 1.8). Platinum sensing elements are fabricated to a boundary layer type probe-body geometry (*Dantec 55P15*) with prong spacings of 3 mm. Wollaston wires are soldered to the prong tips and etched to give a 5μm platinum filament of length approximately 1 mm. Based on recommendations by Ligrani and Bradshaw (7) and Hutchins *et al* (5), the length-to-diameter ratio of the etched hot-wire sensors were set to exceed 200 to minimize attenuation due

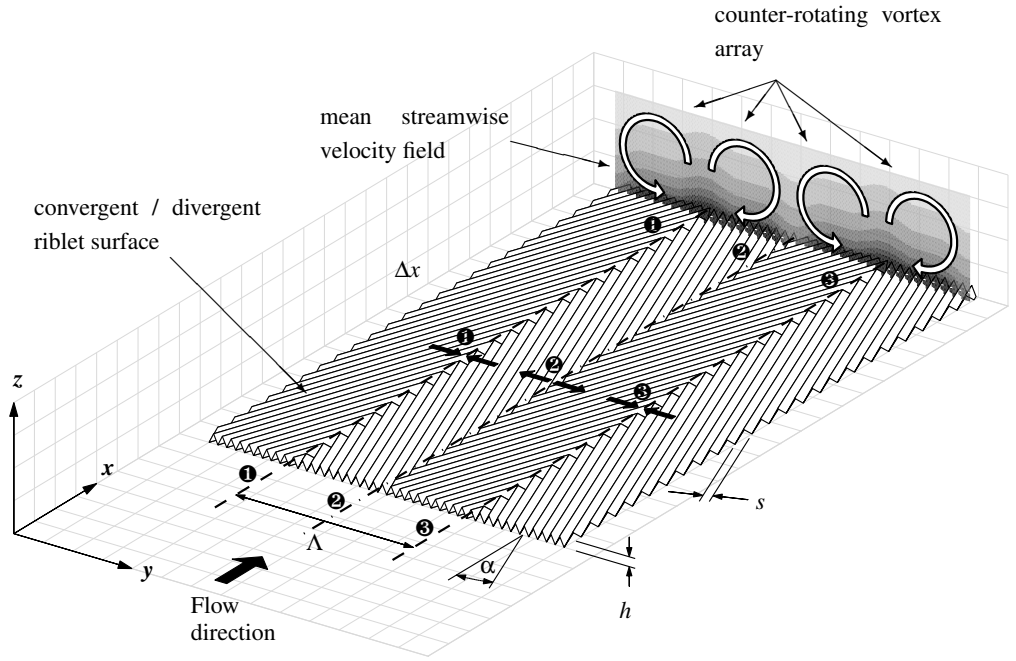

Figure 1: Schematic diagram of converging / diverging riblet pattern, showing expected regions of converging (regions ① and ③) and diverging (region ②) spanwise flow. Contours on the vertical plane show schematic of modification to mean streamwise velocity (dark is low speed, light is high).

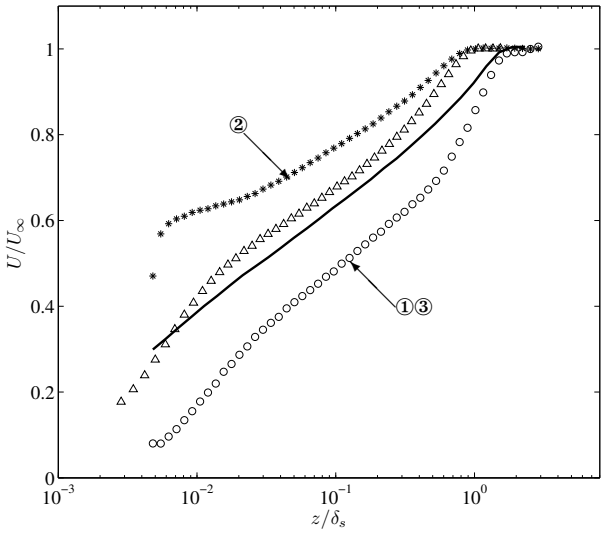

Figure 2: Mean velocity profile over the diverging (∗) and converging (○) regions of the rough surface, and for the smooth wall case (Δ). The solid line represent the averaged spanwise velocity profile over one full wavelength of converging-deverging-converging regionsΛ. Data are non-dimensionalised using boundary layer thickness over the smooth surface (δ_s).

to end conduction. These two studies (7; 5) would indicate that the current sensors (which have viscous-scaled length $l^+ \approx 35$), will suffer some attenuation due to insufficient spatial resolution. However, since at this stage these measurements are made for comparative purposes only (between the smooth wall and riblet modified flows), such attenuation is deemed acceptable. In the following sections, the converging / diverging riblet results will be compared to the smooth wall case for the same freestream velocity.

Results

In each spanwise location, boundary layer traverses of 50 log-

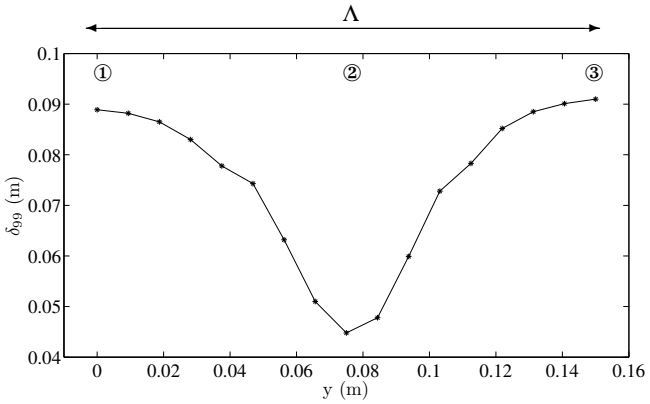

Figure 3: Change of δ_{99} over one spanwise wavelength of the converging-diverging surface.

arithmically spaced measurements were made from 0.25 mm above the peak roughness height up to 120 mm. Table 1 shows boundary layer parameters for the smooth and rough surfaces. Note that for the rough case, owing to the three-dimensionality induced by the riblet patterns, these parameters are local (i.e calculated from profiles at that particular spanwise location). U_∞ is free stream velocity, δ_{99} is boundary layer thickness based on 99% of free stream velocity, δ^* is displacement thickness, θ_m is momentum thickness, H is shape factor, and Re_θ is Reynolds number based on momentum thickness.

Figure 2 shows the mean velocity profiles for the smooth case, and above the converging and diverging regions of the riblet pattern. Note that the wall-normal ordinate is made non-dimensional using boundary layer thickness over the smooth surface (δ_s). It is immediately obvious from this figure that the boundary layer thickness in the converging region is much greater than for the diverging regions and the smooth surface (by a factor of almost two). Figure 3 shows the change in boundary layer thickness over one complete wavelength of the converging-diverging surface roughness. It is perhaps surprising that surface modifications with a protrusion height of approximately 0.5 mm can cause such a pronounced three-dimensionality in the turbulent boundary layer (i.e these very

Surface	U_∞ (ms^{-1})	δ_{99} (m)	δ^* (m)	θ_m	H	Re_θ
smooth	14.24	0.0520	0.0074	0.0055	1.345	5021
diverging ②	14.70	0.0414	0.0046	0.0037	1.239	3455
converging ①③	14.80	0.0887	0.0185	0.0119	1.556	11130

Table 1: Experimental parameters for smooth, diverging, and converging surface.

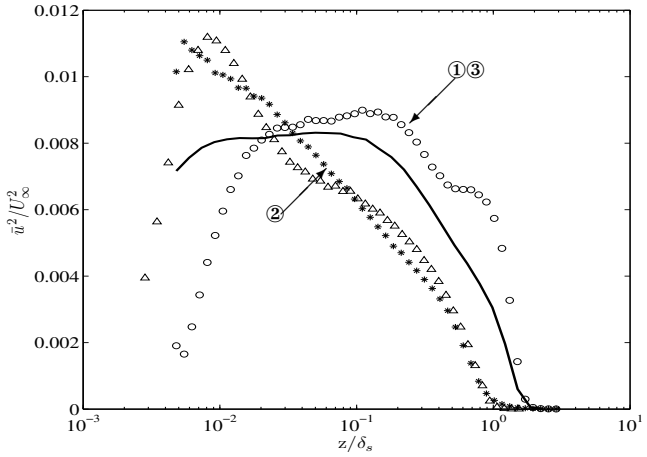

Figure 4: Turbulence intensity profiles over the diverging (∗) and converging (○) regions of the rough surface, and for the smooth wall case (Δ). The solid line is averaged spanwise turbulent intensity over one full wavelength of converging-devergingconverging regions Λ.

small surface perturbations are able to produce greater than 100% spanwise variation in the boundary layer thickness). Figure 2 indicates that the average local velocity above the diverging region is in general higher than the smooth wall velocity. The opposite situation occurs over the converging region of the surface where the local velocity is relatively lower than the smooth wall case. This is as expected since the converging regions ① and ③, will induce the vertical ejection of low-speed fluid away from the wall leading to lowered local streamwise velocities. Conversely, the diverging region ② will induce vertical flow towards the wall causing locally elevated mean streamwise velocities in this region.

The turbulent intensity profiles (figure 4) shows that close to the wall, the turbulent intensity is highly reduced over the converging region and only slightly modified over the diverging region as compared to the smooth wall case. Beyond $z/\delta_s = 0.02$, the turbulent intensity of the converging region climbs above that of the smooth wall case. One possible interpretation of this is that the upwelling caused by the converging pattern, redistributes the near-wall turbulence intensity (which is generally high) into the logarithmic and outer regions of the boundary layer.

Figure 5 shows pre-multiplied spectra maps for smooth, diverging and converging regions. These plots show the magnitude of the pre-multiplied energy spectra (shown by the shaded contours) as a function of streamwise wavelength λ (y axis) and wall-normal location (x axis). Previously it has been shown (4) that canonical ZPG boundary layers exhibit two local peaks in this spectral surface; an inner peak located at ($z^+ = 15$, $\lambda_x^+ = 1000$) due to the near-wall cycle of streaks and quasi-streamwise vortices (Schoppa and Hussain (8)), and an outer peak due to superstructure type events occurring at ($z/\delta \approx 0.06, \lambda_x/\delta \approx 6$). The locations of these two peaks are indicated on the smooth wall plot by the '+' symbols. Note that the outer peak grows in magnitude with Reynolds numbers and for these

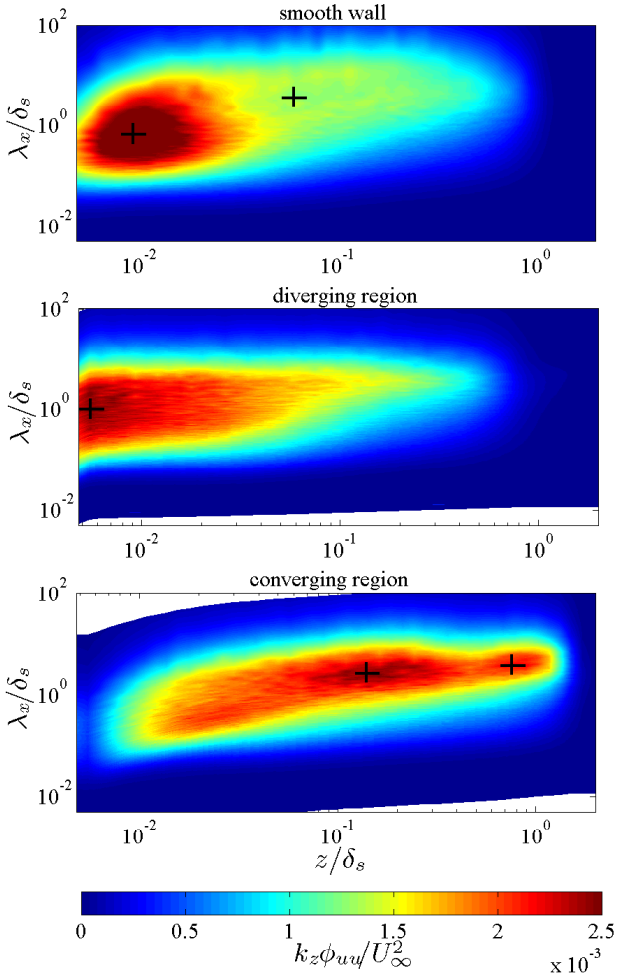

Figure 5: Contours showing pre-multiplied streamwise energy spectra ($k_x\phi_{uu}$) as a function of wall-normal position (z) and energetic streamwise length-scale (λ). Plots are shown for the smooth wall case (top) and above the diverging (center) and converging (bottom) regions. Contour colour scale indicates magnitude of $k_x\phi_{uu}/U_\infty^2$ (k_x is streamwise wavenumber and ϕ_{uu} is the energy spectra of streamwise velocity fluctuations).

(quite low) Reynolds numbers, is not yet fully formed. The spectral surfaces measured over the diverging and converging regions of the riblet patterns in general exhibit few of the features associated with canonical smooth-wall turbulent boundary layers. Over the diverging region, a weak peak occurs close to the wall, but for most of the outer regions ($0.05 < z/\delta_s < 1.3$) the spectral distribution seems to settle into a broad ridge centered at $\lambda_x/\delta_s \approx 3$. Above the converging region, the surfaces are again very different. There is no apparent near-wall peak (which would seem to indicate a radical interruption or redistribution of the near-wall cycle). Instead two broad outer peaks occur, one at ($z/\delta_s \approx 0.15$, $\lambda_x/\delta_s \approx 3$), and a second peak located at ($z/\delta_s \approx 0.8$, $\lambda_x/\delta_s \approx 5$). It appears from these plots that the very largest superstructure type events may have been locked in position over the converging regions of the surface

pattern (and forced further away from the wall). Confirmation of this hypothesis must await PIV measurements or hot-wire rake surveys (as conducted in ref (4)) above the riblet surfaces.

Results on Spanwise Analysis

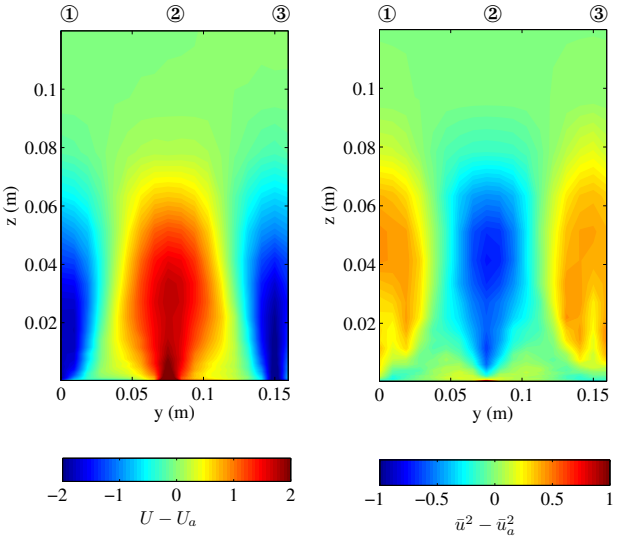

Figure 6: Figures showing the spanwise variation of (a) mean velocity U and (b) turbulence intensity $\overline{u}^2$, as compared to spanwise averaged results (U_a and $\overline{u_a}^2$) results.

Figure 6 shows variation in mean velocity (a) and turbulence intensity (b) for the complete spanwise-wall normal measurement domain. These plots cover one complete wavelength (see dimension Λ in figure 1) of the converging diverging riblet pattern. Note that a diverging region is located at the spanwise midpoint of these figures ($y = 0.074$ m) and converging regions are located at the left and right edges ($y = 0$ and $y = 0.148$ m). Figure 6(a) shows that higher speed regions form above the diverging regions and lower speed regions form above converging surface patterns. Such results are consistent with the findings of Koeltzsch *et al* (6). It appears that the diverging surface patterns cause flow to be swept towards the wall (bringing high momentum fluid from the outer regions into near-wall proximity), whilst the converging regions cause an upwelling from the wall, transporting low-speed near-wall fluid into the outer regions. Such a scenario is also consistent with the turbulence intensity results shown in Figure 6(b), with the smooth wall intensity profile being redistributed by the locally ejecting and sweeping flows located above the converging and diverging regions respectively. In general it is supposed that the converging-diverging surface patterns are generating counter-rotating vortical flows (as sketched in figure 1). Proof of this hypothesis must await measurements of secondary flow components (either with PIV or multi-sensor hot-wires).

Conclusion

A preliminary study has been conducted of a ZPG turbulent boundary layer over a diverging-converging riblet surface. The flow over the diverging surface experiences an increase in local velocity and decrease of the turbulent intensity. Over the converging regions, the opposite scenario occurs, with slower local velocities and a greater turbulent intensity. In general, it is proposed that these changes are consistent with the hypothesis that these highly directional rough surfaces are generating large-scale counter-rotating vortical flows within the turbulent boundary layer, with common-flow-up occurring at the converging regions, and common-flow-down occurring at diverging regions. Analysis of the pre-multiplied energy spectra reveal that the surfaces have radically altered the spectral content of the flow. The high degree of three-dimensionality imposed by the these surfaces is clear both from these energy spectra results and more detailed spanwise surveys of velocity. Based on these results, it is tentatively proposed that the secondary flows induced by these unique surfaces may act to lock the largest-scale motions above the converging regions of the surface. This hypothesis currently lacks solid experimental proof, but does provide some explanation for the observed three-dimensionality.

Although these data are preliminary, they do seem to suggest that this unique surface preparation is generating counter-rotating vortex arrays, and hence these surface patterns could find application in flow control as a 'low-profile' vortex generator. Future analysis will involve a more detailed parametric study of these surfaces, investigating the effect of roughness angle, spanwise wavelength(λ) and development length of the boundary layers developing over these surfaces. We also plan to investigate and characterise the secondary flows (counter-rotating vortex arrays) that we believe these surfaces produce. At this stage, we are not in a position to comment on the effect of the converging-diverging riblet arrangements on the turbulent skin friction, although a preliminary investigation seems to indicate that the wall friction velocity has been increased due to this surface. *

References

[1] Bechert, D. and Bartenwerfer, M., The viscous flow on surfaces with longitudinal ribs, *J. Fluid Mech.*, **206**, 1989, 105–129.

[2] Bechert, D., Bruse, M., Hage, W., Van Der Hoeven, J. G. and Hoppe, G., Experiments on drag-reducing surfaces and their optimisation with an adjustable geometry, *J. Fluid Mech.*, **338**, 1997, 59–87.

[3] Choi, K.-S., Near-wall structure of a turbulent boundary layer with riblets, *J. Fluid Mech.*, **208**, 1993, 417–458.

[4] Hutchins, N. and Marusic, I., Evidence of very long meandering features in the logarithmic region of turbulent boundary layers, *J. Fluid Mech.*, **579**, 2007, 1–28.

[5] Hutchins, N., Nickels, T. B., Marusic, I. and Chong, M. S., Hot-wire spatial resolution issues in wall-bounded turbulence., *J. Fluid Mech.*, **635**, 2009, 103–136.

[6] Koeltzsch, K., Dinkelacker, A. and Grundmann, R., Flow over convergent and divergent wall riblets, *Exp. Fluids*, **33**, 2002, 346–350.

[7] Ligrani, P. M. and Bradshaw, P., Spatial resolution and measurement of turbulence in the viscous sublayer using subminiature hot-wire probes, *Exp. Fluids*, **5**, 1987, 407–417.

[8] Schoppa, W. and Hussain, F., Coherent structure generation in near-wall turbulence, *J. Fluid Mech.*, **453**, 2002, 57–108.

[9] Walsh, M. J., Riblets as a viscous drag reduction technique, *AIAA Journal*, **21 4**, 1983, 485–486.